The annual cycle of hydrogen peroxide: an indicator of chemical instability?

R. W. Stewart

Atmos. Chem. Phys., 4, 933–946, 2004
www.atmos-chem-phys.org/acp/4/933/
SRef-ID: 1680-7324/acp/2004-4-933

Atmospheric Chemistry and Physics

The annual cycle of hydrogen peroxide: an indicator of chemical instability?

R. W. Stewart

NASA Goddard Space Flight Center, Greenbelt, MD 20771, USA

Received: 11 March 2004 – Published in Atmos. Chem. Phys. Discuss.: 6 April 2004
Revised: 9 June 2004 – Accepted: 21 June 2004 – Published: 25 June 2004

Abstract. A box model has been used to study the annual cycle in hydrogen peroxide concentrations with the objective of determining whether the observed difference in summer and winter values reflects instability in the underlying photochemistry. The model is run in both steady-state and time-dependent modes. The steady-state calculations show that, for some range of NO_x background levels, two stable solutions to the continuity equations exist for a period of days in spring and fall. The corresponding time-dependent model indicates that, for sufficiently high background NO_x concentrations, the spring and fall changes in H_2O_2 concentration may be interpreted as a forced transition between the two underlying stable regimes. The spring transition is more rapid than that in fall, an asymmetry that becomes more marked as background NO_x increases. This asymmetry is related to the different time scales involved in chemical production and loss of H_2O_2. Observations of the spring increase in H_2O_2 concentration may therefore provide a better measure of the change in the underlying chemical regime than does the fall decrease. The model results developed in this paper will be compared with two sets of observations that cover annual variations of peroxide concentrations under different background pollution conditions.

1 Introduction

Several publications (e.g. White and Dietz, 1984; Stewart, 1993; Kleinman, 1994) have shown that the continuity equations that describe tropospheric photochemistry can exhibit bifurcations and consequent multiple steady-state solutions. These phenomena occur in the transition region between what may be characterized as low-NO_x and high-NO_x chemical regimes. It is not known whether these mathematical properties exhibited by steady-state models correspond to observable phenomena in the time-dependent world. This paper addresses the question of observable consequences.

Steady-state and time-dependent calculations over an annual cycle are carried out showing that bifurcations in the steady-state solutions have an analogue in the time- dependent case. Above a certain background NO_x level rapid changes in oxidant concentrations occur in time-dependent calculations. These correspond to bifurcations in the steady-state case. The rapidity of the transition increases with increasing background NO_x.

It is obvious that such transitions do not occur on the global scale, a predominately low-NO_x environment. Their importance lies in the fact that, should they occur on more polluted regional scales, they can involve large changes in oxidant levels with a corresponding change in pollutants over a short time period of several days. Hydrogen peroxide, the focus of the discussion in this paper is an especially sensitive indicator of the low-NO_x, high-NO_x transition.

1.1 The observed annual cycle of H_2O_2

This paper will discuss the annual cycle of H_2O_2 in the context of the low-NO_x and high-NO_x chemical regimes described by Kleinman (1991). A basic difference in these regimes is the concentration and fate of oxidants. In the high-NO_x regime OH reacts predominantly with NO_2 to form nitric acid. Nitric acid is mostly removed by deposition before it can react to return its components to the atmosphere and its formation is thus a permanent loss for odd hydrogen (HO_x=OH+HO_2). Since H_2O_2 is formed through reaction of two HO_2 radicals it is particularly sensitive to the changes in concentration of HO_x components that occur in the transition from low-NO_x to high-NO_x conditions. We will explore the possibility that observed mixing ratio changes in the tropospheric boundary layer might, under some circumstances, be interpreted as resulting from instability in the underlying

Correspondence to: R. W. Stewart
(Richard.W.Stewart@nasa.gov)

steady-state chemistry. Due to the sensitivity of hydrogen peroxide to such instability it is reasonable to concentrate on its annual cycle.

Most measurements of H_2O_2 have been made over relatively limited time spans (see the review by Lee et al. (2000)). Measurements of peroxide over an annual cycle have been made by Ayers et al. (1996) at Cape Grim, Tasmania (41° S) and Sakugawa and Kaplan (1989) in and near Los Angeles, CA. The Ayers et al. (1996) measurements are of H_2O_2 plus organic peroxide and represent unpolluted marine air. They show monthly means varying from 0.16 to 1.4 ppb. The Sakugawa and Kaplan measurements of H_2O_2 were carried out in a more polluted environment. Measurements of Gnauk et al. (1997) were carried out over a 3-year period, but are only reported for selected days or over short intervals. Peroxide observations were made over a four-month period during the Tropospheric Ozone Production about the Spring Equinox (TOPSE) experiment (Snow et al., 2003). Although this time period is of special interest to the present study, the NO_x mixing ratios were too low to contribute to low to high-NO_x transitions (Snow et al., 2003; Tie et al., 2003).

The body of observations covers different locations and times of year and is useful for deducing general characteristics of the annual cycle of H_2O_2. The property of the H_2O_2 annual cycle of most interest in this study is the change from a winter minimum to a summer maximum under various levels of background pollution as represented by the NO_x mixing ratio. The annual cycle observations of Ayers et al. (1996) and Sakugawa and Kaplan (1989) are most relevant to this study and will be discussed after model results are presented.

1.2 Nonlinearities

The nonlinearity of the continuity equations describing atmospheric photochemistry gives rise to a number of interesting consequences. This paper will focus on multiple solutions in tropospheric models, but these have also been discussed with regard to the stratosphere (Prather et al., 1979; Fox et al., 1982; Konovalov et al., 1999) and mesosphere (Yang and Brasseur, 1994).

A relatively simple consequence of nonlinearity that has been discussed in the context of tropospheric models for some time is "turnaround" behavior. This refers to a change in sign of the rate of change of a species concentration, such as ozone, with respect to a monotonically changing control parameter, such as a nitric oxide source. Stewart et al. (1977) described the change in O_3 response with increasing NO_x emission. They showed that $[O_3]$ first increased, then decreased as NO emission increased, with a turnaround occurring when the NO_x background reached roughly 500 ppt. Hameed et al. (1979) discussed the importance of the NO_x background on OH behavior and on the effect of increased CO source levels in the troposphere. The hydroxyl radical, like ozone, exhibits a turnaround as we go from a low to a high-NO_x background. It was shown that an increasing CO source could either increase OH and decrease CH_4 or have the opposite effect as NO_x background changes. Poppe et al. (1993) discussed the nonlinear OH response to changes in several model parameters.

White and Dietz (1984) were the first to describe a more startling aspect of nonlinearity in a tropospheric model, the existence of multiple steady states. These authors showed that the NO_x removal rate is a non-monotonic function of NO_x concentration. This implies that multiple concentration values can exist over a critical range of NO_x emission rates. Stewart (1993, 1995) described methods for computing multiple solutions and exhibited them for a variety of assumptions regarding both the reactions included in a model and the source values for key species. Multiple solutions occur when a control parameter, typically NO source, is varied past a critical value at which a bifurcation from one to three solutions occurs. Further variation in the same direction leads to another bifurcation in which the number of solutions is reduced to one. These bifurcation points bound a bistable region in the state space of the system, i. e., a region in which two stable steady states exist. It has not been clear how, or if, the bistability exhibited in simple models relates to observable phenomena. Kleinman (1991) suggested that the difference in summer and winter H_2O_2 concentrations observed in the northeastern United States might reflect the difference in underlying low-NO_x (summer) and high-NO_x (winter) photochemical states. Jacob et al. (1995) suggest that measurement of H_2O_2, and several other species, show evidence of a September transition from low-NO_x (NO_x-limited) to high-NO_x (hydrocarbon-limited) conditions. Their data, along with other observations noted in the paper, suggest a roughly factor of 5 decrease in H_2O_2 during September.

1.3 Chemical instability

The terms "chemical instability" and "unstable solution" are used throughout this paper. Both steady-state and time-dependent solutions of continuity equations are presented to illustrate the phenomena described by these terms and possible atmospheric consequences of such phenomena. For corresponding parameter values, the steady-state solutions are expected to serve as "attractors" for the time-dependent model. For example, the solutions of a diurnally forced model should remain close to the corresponding solutions of a diurnally averaged one. In this sense, steady-state models can provide an approximation to averaged conditions in the atmosphere. An exception occurs if the steady-state solution is unstable.

An unstable solution refers to a steady-state model in which the Jacobian matrix, evaluated at a solution, has at least one eigenvalue with a positive real part. The Newton-Raphson method used in solving the steady-state model (Stewart, 1993) uses the Jacobian, but not its eigenvalues. In a steady-state model there is thus no computational

difference between stable and unstable solutions. If we now solve the same equations, but use a time-dependent method to study the behavior of the solutions near a steady state, the Jacobian eigenvalues appear as arguments of exponential functions that describe the model's temporal evolution. If the real parts of all eigenvalues are negative, the solution simply relaxes to the steady state, but any positive real part will drive the time-dependent solution away from the steady state. This is the meaning of instability and the consequence is that unstable steady-state solutions are inaccessible to a time-dependent model and cannot provide an approximation to conditions in the atmosphere.

Our interest in instability is in determining how a time-dependent model behaves when underlying steady-state attractors, differing only by a small value of a parameter, are nonetheless widely separated in the state space of the system. This will occur in bistable regions referred to above. An example in the following is provided by steady states calculated on successive days of the year. The small change in solar zenith angle that this entails will, under some conditions, result in large changes in species concentrations. When these steady-state changes have a time-dependent analog we expect that, to the extent that the time-dependent model provides some approximation to the atmosphere, there may be observable consequences.

2 Background

2.1 Tropospheric chemical regimes

In both stratosphere and troposphere the source of ozone is molecular oxygen. In the stratosphere a single UV photon having wavelength $\lambda \leq 242$ nm suffices to dissociate molecular oxygen and form O_3 via reaction of the product O atoms with O_2. Since these photons do not penetrate to the troposphere, ozone production utilizes two less energetic photons and a more involved sequence of chemical reactions. The first photon, $\lambda \leq 340$ nm, photolyzes a seed molecule of O_3 yielding an excited-state oxygen atom, $O(^1D)$. This may then react with water vapor to form OH. OH oxidation of a hydrocarbon (HC), represented by CO and CH_4 in the following, releases H atoms or methyl radicals, respectively. These capture O_2 to form HO_2 or CH_3O_2 and, with sufficient NO present, an O atom is subsequently transferred to NO forming NO_2. The second photon, $\lambda \leq 423$ nm, now photolyzes NO_2 releasing O to form O_3 as in the stratosphere. Since this process only consumes HC and H_2O and not NO_x or HO_x there is no need for further O_3 photolysis to continue O_3 production. Ozone in the troposphere is thus its own precursor and its production is autocatalytic (Stewart, 1995). These ideas are elaborated in the remainder of this section.

A simplified photochemical scheme will be used to illustrate the behavior of the model used in this study. Such a simplification is often used to demonstrate basic properties of tropospheric chemistry and variants have appeared often in the literature (Tinsley and Field, 2001; Field et al., 2001; Kalachev and Field, 2001; Prather, 1994). The actual model chemistry is described later, but the simplified scheme will be a useful reference for interpreting model results and understanding conditions in which bifurcations in the steady-state model and low-NO_x , high-NO_x transitions in the time-dependent model occur. Many authors have discussed the reactions described below (e.g. Levy, 1971; Crutzen and Zimmermann, 1991; Kleinman, 1991; Lelieveld et al., 2002).

The photochemical system may be regarded as consisting of three sets described as follows: 1) Initiation, 2) Chain propagation, and 3) Termination.

2.1.1 Initiation

The initiation phase begins with the photolysis of an ozone molecule by solar UV radiation in the 300–340 nm range. This produces excited-state $O(^1D)$ atoms, some of which react with water vapor to form two OH radicals. These initial reactions may result in ozone loss or production, depending on subsequent reactions.

$$O_3 + h\nu \rightarrow O(^1D) + O_2 \quad (1)$$

$$O(^1D) + H_2O \rightarrow 2OH \quad (2)$$

2.1.2 Chain propagation

The fate of oxidants after the initiation phase begins with oxidation of CO. Carbon monoxide serves here as a surrogate for CH_4 and other hydrocarbon species. Since NO_x and HO_x are not consumed in the following they are referred to collectively as chain propagation reactions.

$$CO + OH + O_2 \rightarrow HO_2 + CO_2 \quad (3)$$

$$HO_2 + NO \rightarrow NO_2 + OH \quad (4a)$$

$$HO_2 + O_3 \rightarrow OH + 2O_2 \quad (4b)$$

$$NO_2 + O_2 + h\nu \rightarrow NO + O_3 \quad (5)$$

2.1.3 Termination

For simplicity only the following chain termination reactions are considered.

$$OH + NO_2 + M \rightarrow HNO_3 + M \quad (6)$$

$$HO_2 + HO_2 \rightarrow H_2O_2 + O_2 \quad (7)$$

In a low-NO_x regime the net chemistry may result in either ozone loss or production. If it results in production, large numbers of ozone molecules may be produced for each one initially photolyzed. Depending on the amount of CO or hydrocarbon (HC) available Reactions (3–5) may occur several times before a termination reaction occurs that removes radicals or NO_x from the system. Suppose that Reactions (3–5)

Table 1. Variable species included in the present model.

No.	Species	Flux ($cm^{-2}\,s^{-1}$)	Dep. Velocity (cm/s)
1	O_3	7×10^{10}	0.4
2	OH		
3	HO_2		
4	H_2O_2		0.50
5	NO	variable	0.016
6	NO_2		0.10
7	HNO_3		4.0
8	CO	1×10^{11}	0.03
9	CH_3OOH		0.1
10	CH_3O_2		
11	CH_2OOH		
12	H_2CO		0.25
13	CH_3OH		
14	NO_3		0.1
15	N_2O_5		4.0
16	HNO_2		
17	HNO_4		4.0
18	C_2H_4	2×10^9	
19	$C_2H_4OHO_2$		
20	C_2H_4OOH		
21	CH_2O_2		
22	C_2H_6	2×10^9	
23	$C_2H_5O_2$		
24	CH_3CHO		0.25
25	CH_3CO_3		
26	PAN		

occur m times before a termination reaction occurs. Further, within this sequence, suppose that Reaction (4a) occurs m_1 times and Reaction (4b) m_2 times with m_1+m_2=m. Then the net effect of Reactions (1–5) is:

2.1.4 Net

$$O_3 + H_2O + mCO + (2m_1 - m_2 - 1)O_2 \rightarrow mCO_2 + 2OH + (m_1 - m_2)O_3 \quad (8)$$

The above system behaves in the following way.

Net Production of O_3: $m_1 > m_2+1$
O_3 neutral: $m_1 = m_2+1$
Net destruction of O_3: $m_1 < m_2+1$

The transition from ozone destruction to ozone production in the low-NO_x regime occurs when the reaction rates (4a) and (4b) are approximately equal, i.e. $k_{4b}[O_3] \approx k_{4a}[NO]$.

Once there is sufficient NO in the system to provide net chemical production, we see from the net reaction that this production is autocatalytic with m_1–m_2 ozone molecules produced for each one destroyed. For CH_4 or NMHC consumption, the potential ozone production is greater, but details will not be considered here.

Dominance of Reaction (4b) over (4a), if it occurs, does not imply that HO_2+O_3 is itself a major ozone loss mechanism. The competition between O_3 and NO for HO_2 simply provides a switch that, if O_3 is favored, allows ozone photolysis to act as the principal ozone loss mechanism rather than as the first step in the autocatalytic production of ozone. This process was described as inhibition (of ozone production) in Stewart (1995).

The effects of these reactions are summarized in Fig. 1. The circles represent species playing the role of sources (HC) or sinks (H_2O_2 and HNO_3) for the more reactive species shown in the boxes. In this figure, the light-blue boxes and circles and dark-blue arrows indicate the chemistry of the low-NO_x, ozone loss regime. OH production through Reactions (1) and (2) is followed by conversion to HO_2 via hydrocarbon oxidation and then loss of HO_x and O_3 after Reaction (7) forms peroxide. The path Reaction (3) followed by Reaction (7) shows the loss of ozone and odd hydrogen. Net production of oxidants does not occur in this system.

Adding NO_x to the system provides the mechanism for autocatalytic production of ozone. This is shown by adding the brown boxes and green arrows in Fig. 1. The dotted green arrows in the diagram show the recycling of NO_x and HO_x. The arrows connected to small filled circles in the HO_2 box indicate the alternate pathways that may be followed by HO_2. The low-NO_x switch from ozone loss to production occurs when the Reaction (4a) path dominates Reaction (4b) as described above.

Finally, when enough NO_x is present, OH will react preferentially with NO_2 to form nitric acid. This establishes the high-NO_x regime shown by adding the red circle (HNO_3) and arrows on the left side of Fig. 1. Once this occurs the low-NO_x paths on the right of the figure are substantially shut down and production of oxidants, including H_2O_2, becomes negligible. The small filled circles in the OH box indicate the switch between low and high-NO_x chemistry.

2.2 Model description

2.2.1 Methods and Parameters

Many model details are the same as described in Stewart (1993, 1995). A box model (Stewart, et al., 1983) is used to compute species concentrations. A Newton-Raphson method (Press et al., 1992), modified to enhance its robustness (Stewart, 1993), is used to compute steady-state solutions and the LSODE integrator (Hindmarsh, 1983) is used for time-dependent runs. Methane is held fixed at a mixing ratio of 1.7 ppm. Temperature is assumed to vary through the year from 273K to 297K similar to the model of Kleinman (1991). Water vapor varies with an annual cycle consistent with the temperature change and the assumption of a fixed 60% relative humidity. Fixed ozone burdens of 300 D.U. and

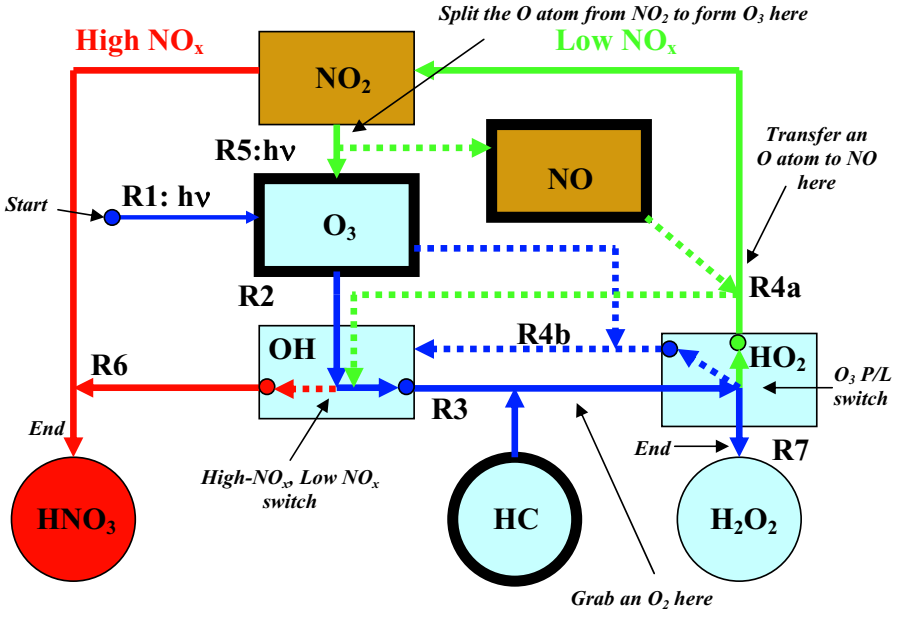

Fig. 1. Diagram illustrating the effects of the basic Reactions (1–7). Boxes bounded by thick lines indicate species having physical sources. The differently colored boxes and arrows indicate Low-NO_x ozone loss (blue), low-NO_x ozone production (blue and brown) and high-NO_x (red) regimes.

boundary layer height of 1 km. have been used in the results reported below. Test calculations have been made with annual variations of these last parameters, but without significant change in the results.

There are 26 variable species (Table 1) undergoing 65 reactions (Table 2). In addition to their chemical interactions, several species shown in Table 1 are assumed to have physical sources and/or sinks. The physical source of O_3 is transport from the stratosphere. The mean value used for the O_3 flux is in the range discussed by Holton and Lelieveld (1994). The CO source is based on a global anthropogenic source value (Olivier et al., 1999). Sources for ethene and ethane are assumed that give values of these species consistent with observations (Bottenheim and Shepherd, 1995) over some range of model runs. Except for H_2CO, deposition velocities are from the model study of Hauglustaine et al. (1994). The formaldehyde deposition rate is assumed the same as that for CH_3CHO. In all cases fluxes and deposition velocities are converted to sources and loss coefficients by dividing by the boundary layer height of 1 km. No other exchange processes, such as coupling to a specified ambient atmosphere, are considered in this model.

Some experimentation has been carried out with all of these model parameters. The main qualitative features discussed below, namely the existence of spring and fall transitions between high and low-NO_x regimes in both steady-state and time-dependent models, have not been sensitive to the values used.

2.2.2 Chemistry

Table 2 presents the chemical reactions used in this study. Photolysis rates are computed from the Madronich (1987) model for clear sky conditions at 40° N. Reaction rates are mostly taken from Demore et al. (1997) and Atkinson et al. (1992). A few tests were made with updated values given in the compilation of Sander et al. (2003) with no significant change in results. Some of the reactions in Table 2 have products that react with O_2. In such cases, the products shown are those subsequent to the O_2 reaction. Reaction (1) showing ozone yielding OH directly is a composite reaction having an effective rate coefficient that depends on water vapor concentration as well as total number density. The effective rate is similar to that discussed in Stewart (1995), but is now treated as a photolysis rate rather than a bimolecular rate involving H_2O. Hydrolysis of N_2O_5 (Reaction 41 in Table 2) follows the discussion of Dimitroulopoulou and Marsh (1997) using an effective rate that accounts for both heterogeneous and homogeneous reactions. Reactions (50) and (51) following the oxidation of C_2H_4 by OH (Reaction 49) are based on the oxidation sequence given in Barker (1995). The rate for Reaction (50) is a guess taken to be of a magnitude similar to the rates for HO_2+NO and CH_3O_2+NO. The thermolysis rate for Reaction (51) is also a guess taken to be the same as the rate for HNO_4 thermolysis. The Reactions (52) and (53) are based on Barker (1995) as well as the discussion of Paulson (1995).

Table 2. Reactions used in the current model. The temperature used for rate evaluation is 278 K. This is the temperature at noon on 1 January in the model. Rate numbers in parentheses correspond to the numbers in Sect. 2.1

No.	Name	Rate($cm^3\ s^{-1}$)
R1 (R1+R2)	$O_3 + h\nu \rightarrow 2OH$	2.03D-07
R2 (R5)	$NO_2+h\nu \rightarrow NO+O_3$	6.42D-03
R3	$H_2O_2+h\nu \rightarrow OH+OH$	3.45D-06
R4	$HNO_3+h\nu \rightarrow OH+NO_2$	1.97D-07
R5	$PAN+h\nu \rightarrow CH_3CO_3+NO_2$	2.10D-07
R6	$OH+HO_2 \rightarrow H_2O+O_2$	1.18D-10
R7	$H_2O_2+OH \rightarrow HO_2+H_2O$	1.63D-12
R8	$OH+O_3 \rightarrow HO_2+O_2$	5.45D-14
R9 (R4b)	$HO_2+O_3 \rightarrow OH+2O_2$	1.82D-15
R10 (R4a)	$NO+HO_2 \rightarrow OH+NO_2$	8.60D-12
R11	$NO+O_3 \rightarrow NO_2+O_2$	1.30D-14
R12 (R3)	$CO+OH \rightarrow CO_2+HO_2$	2.44D-13
R13	$OH+OH+M \rightarrow H_2O_2+M$	6.15D-12
R14 (R6)	$OH+NO_2+M \rightarrow HNO_3+M$	1.05D-11
R15 (R7)	$HO_2+HO_2+M \rightarrow H_2O_2+O_2+M$	5.33D-12
R16	$H_2CO+h\nu \rightarrow 2HO_2+CO$	1.66D-05
R17	$H_2CO+h\nu \rightarrow CO+H_2$	2.80D-05
R18	$CH_3OOH+h\nu \rightarrow CH_3O_2+OH$	3.10D-06
R19	$CH_4+OH \rightarrow CH_3O_2+H_2O$	4.15D-15
R20	$CH_3O_2+HO_2 \rightarrow CH_3OOH+O_2$	6.74D-12
R21	$CH_3OOH+OH \rightarrow CH_3O_2+H_2O$	5.46D-12
R22	$CH_3OOH+OH \rightarrow CH_2OOH+H_2O$	2.30D-12
R23	$CH_2OOH+M \rightarrow H_2CO+OH$	1.00D-12
R24	$CH_3O_2+CH_3O_2 \rightarrow 2H_2CO+2HO_2$	1.95D-13
R25	$CH_3O_2+CH_3O_2 \rightarrow H_2CO+CH_3OH+O_2$	2.92D-13
R26	$CH_3OH+OH \rightarrow H_2O+CH_3O_2$	8.15D-13
R27	$NO+CH_3O_2 \rightarrow NO_2+H_2CO+HO_2$	8.21D-12
R28	$H_2CO+OH \rightarrow CO+HO_2$	1.00D-11
R29	$NO_3+h\nu \rightarrow NO_2+O_3$	1.56D-01
R30	$NO_3+h\nu \rightarrow NO+O_2$	2.04D-02
R31	$N_2O_5+h\nu \rightarrow NO_2+NO_3$	1.23D-05
R32	$HNO_3+OH \rightarrow NO_3+H_2O$	1.96D-13
R33	$NO_2+O_3 \rightarrow NO_3+O_2$	1.80D-17
R34	$NO_3+NO_2 \rightarrow NO+NO_2+O_2$	5.39D-16
R35	$NO_3+NO \rightarrow 2NO_2$	2.76D-11
R36	$NO_3+NO_3 \rightarrow 2NO_2+O_2$	1.56D-16
R37	$OH+NO_3 \rightarrow HO_2+NO_2$	2.30D-11
R38	$HO_2+NO_3 \rightarrow HNO_3+O_2$	2.05D-12
R39	$HO_2+NO_3 \rightarrow OH+NO_2+O_2$	3.55D-12
R40	$NO_3+H_2CO \rightarrow HNO_3+HO_2+CO$	4.32D-16
R41	$N_2O_5+H_2O \rightarrow HNO_3+HNO_3$	9.85D-22
R42	$NO_3+NO_2+M \rightarrow N_2O_5+M$	1.35D-12
R43	$N_2O_5 \rightarrow NO_3+NO_2$	3.97D-03
R44	$HNO_2+h\nu \rightarrow OH+NO$	2.50D-03
R45	$HNO_4+h\nu \rightarrow HO_2+NO_2$	2.03D-06
R46	$NO_2+HO_2+M \rightarrow HNO_4+M$	1.62D-12
R47	$OH+NO+M \rightarrow HNO_2+M$	7.90D-12
R48	$HNO_4 \rightarrow HO_2+NO_2$	8.21D-03
R49	$C_2H_4+OH+M \rightarrow C_2H_4OHO_2$	8.16D-12
R50	$C_2H_4OHO_2+NO \rightarrow C_2H_4OOH+NO_2$	2.00D-12
R51	$C_2H_4OOH+M \rightarrow 2H_2CO+HO_2$	1.96D-02
R52	$C_2H_4+O_3 \rightarrow H_2CO+CH_2O_2$	5.85D-19
R53	$C_2H_4+O_3 \rightarrow H_2CO+HO_2+OH$	5.85D-19
R54	$CH_2O_2+HO_2 \rightarrow H_2CO+OH$	1.00D-11
R55	$C_2H_6+OH \rightarrow C_2H_5O_2+H_2O$	1.86D-13
R56	$C_2H_5O_2+NO \rightarrow NO_2+HO_2+CH_3CHO$	9.66D-12
R57	$CH_3CHO+h\nu \rightarrow CH_3O_2+HO_2+CO$	2.21D-06
R58	$CH_3CHO+h\nu \rightarrow CH_3CO_3+HO_2$	9.71D-07
R59	$CH_3CHO+OH \rightarrow CH_3CO_3+H_2O$	1.48D-11
R60	$CH_3CHO+NO_3 \rightarrow CH_3CO_3+HNO_3$	1.77D-15
R61	$CH_3CO_3+NO_2 \rightarrow$ PAN	9.70D-12
R62	$PAN \rightarrow CH_3CO_3+NO_2$	2.05D-05
R63	$CH_3CO_3+HO_2 \rightarrow M$	1.51D-11
R64	$CH_3CO_3+CH_3CO_3 \rightarrow 2CH_3O_2$	1.75D-11
R65	$CH_3CO_3+NO \rightarrow NO_2+CH_3O_2$	1.93D-11

3 Results

3.1 The computed annual cycle of H_2O_2

The primary control parameter in this study is the day of the year. Steady-state concentrations for the variable species given in Table 1 are computed on successive days throughout the year using noon photolysis rates multiplied by the daylight fraction. This implies a corresponding small variation in solar zenith angle between runs and it is also reasonable to consider zenith angle as the primary control parameter. The secondary control parameter is the nitric oxide source, S_{NO}. A range of source fluxes from 4×10^9 to $4\times10^{12}\ cm^{-2}\ s^{-1}$ has been used in the calculations. A time-dependent model has been run for a two-year period with annual and diurnal forcing for several of the S_{NO} values used in the steady-state model. The annual cycles of H_2O_2 from the steady-state model and from the second year of the time-dependent model are compared in this section.

In panels (c) and (d) of the following Figs. 2–5, the displayed rates of OH and HO_2 reaction are keyed to the discussion in section 2.1 and the mechanism shown in Fig. 1. In some cases, at the higher NO_x levels, the formation of nitrous or pernitric acid is actually among the top three rates. Rapid photolysis or thermolysis however will make these "do nothing" reactions and their exclusion is justified. In the models displayed in the following figures, reaction of OH with NMHC is not competitive with the rates shown.

Figure 2 shows steady-state calculations (a), the corresponding time-dependent results (b), the time-dependent variation of noon values of OH loss due to reaction with CO and CH_4 and with NO_2 throughout the year (c), and the HO_2 loss due to reactions with NO and O_3 along with the H_2O_2 production rate (d). The NO source value in these calculations is the lowest considered and results in a NO_x background that ranges from about 40 to 80 ppt. A regional

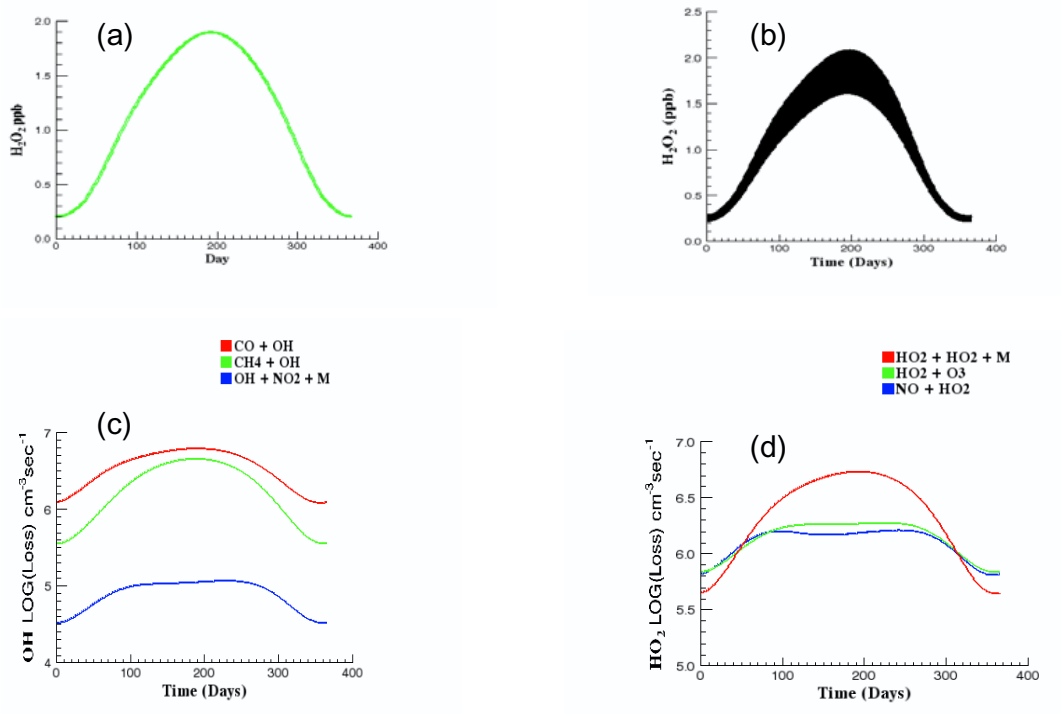

Fig. 2. Steady-state **(a)** and time-dependent **(b)**, **(c)** and **(d)** calculations for the lowest S_{NO} considered. The NO source here is 4×10^4 cm^{-3} s^{-1} and results in a summer to winter range of background NO_x of 40 to 80 ppt. Low NO_x conditions prevail throughout the year as shown by the dominance of CO (red) and CH_4 (green) oxidation over HNO_3 formation (blue) in panel (c). Panel (d) indicates that the net chemistry is ozone destroying throughout the year. The color scheme in parts (c) and (d) is based on the integrated loss by a reaction over an annual cycle, not on the reaction name. In some of the following figures the reactions will be represented by different colors.

characterization based on this range would be remote tropical forest (National Research Council, 1992). This, and similar NRC characterizations noted later, refers only to NO_x levels and not to other aspects of the chemistry. Smaller NO_x sources would result in an annual low-NO_x cycle characteristic of the remote marine troposphere. Both steady-state and time-dependent H_2O_2 mixing ratios vary from a winter low of about .25 ppb to a summer high of about 2 ppb. The annual cycle of H_2O_2 shown in Fig. 2b is qualitatively similar to the observations of Ayers et al. (1996), but with a higher summer maximum as would be expected for higher [NO_x] mixing ratio. Figure 2c indicates that low NO_x conditions prevail throughout the year in this model since nitric acid formation is never competitive with hydrocarbon oxidation. A similar comparison of HO_2 loss rates (d) shows that the chemistry results in net ozone destruction throughout most of the year. In this model ozone photolysis removes odd oxygen and peroxide formation removes odd hydrogen.

The effect of increasing S_{NO} from that used in this model is to depress the winter mixing ratio and increase the summer high. The chemistry remains low-NO_x throughout the year until, at $S_{NO}\approx3.7\times10^5$ cm^{-3} s^{-1}, a narrow region of bistability first appears that spans a single day, 8 February in late winter and 25 November in fall. Further increases in S_{NO} increase the bistable ranges and move their locations towards spring and early fall.

Figure 3 shows the same series of calculations as Fig. 2 with an NO source of 2×10^6 cm^{-3} s^{-1}. This S_{NO} value was chosen because it is in a range characteristic of the northeastern US and is similar to values used by Kleinman (1991) and Jacob et al. (1995). The range of background NO_x mixing ratios in this calculation is 0.5 to 5 ppb, which may be classified as a rural environment (National Research Council, 1992). In this figure, and those following, the H_2O_2units in the steady-state calculation, part (a), will be shown as Log_{10} concentration rather than mixing ratio, as in Fig. 2a, to show the full range of summer to winter variation. Mixing ratios will be retained for the time-dependent profile, Fig. 3b, since this will better exhibit the transitions of interest. The H_2O_2 detection limit depends on measurement method, but is of the order of several to several tens of ppt (Lee et al., 2000). Mixing ratios along the abscissa in Fig. 3b and subsequent figures may be regarded as unobservable.

The steady-state profile, Fig. 3a, now exhibits a mushroom shape (Grey and Scott, 1990). In this model the mushroom results from the symmetry of the spring/fall calculation and consists of two conjoined hysteresis curves. The bistable regions extend from days 78 to 91 in the spring (19 March

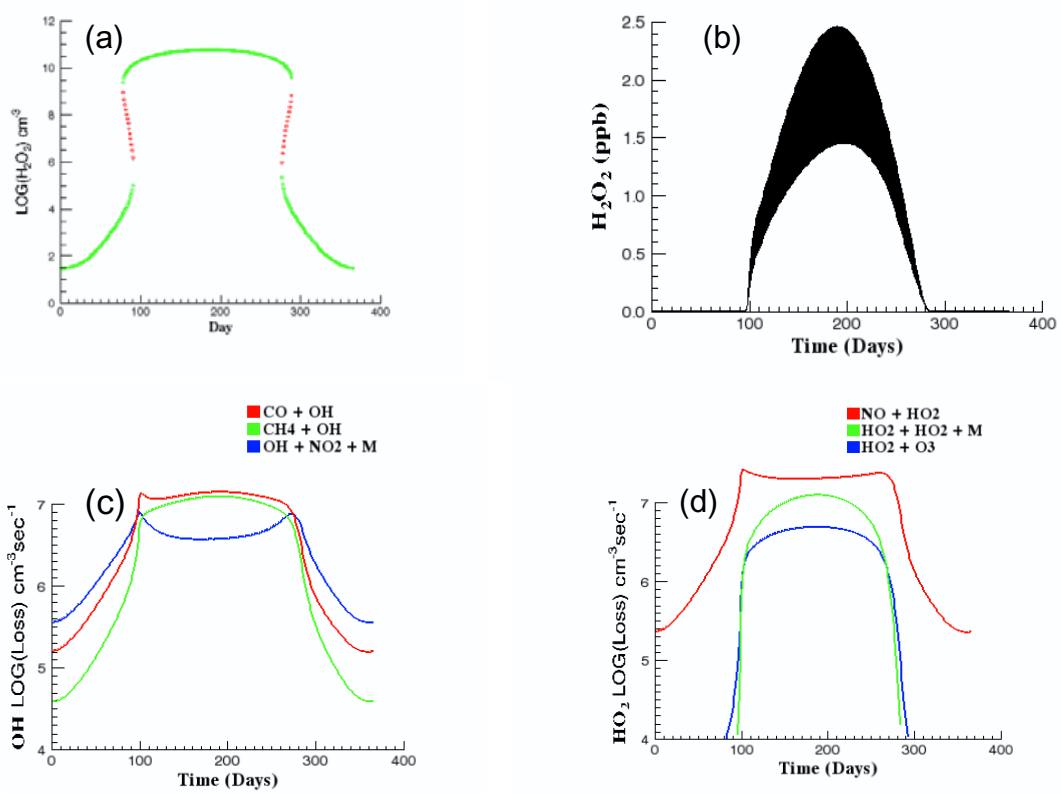

Fig. 3. Steady-state **(a)** and time-dependent **(b)** and **(c)** calculations for S_{NO} of 2×10^6 cm^{-3} s^{-1}. The summer to winter NO_x range in this model is 0.5 to 5 ppb. Part (c) shows that HNO_3 formation (blue) dominates CO (red) and CH_4 (green) oxidation in winter, while panel (d) shows the HO_2 switch (Fig. 1) favors ozone production (red) over loss (blue).

to 1 April) and days 275 to 288 in the fall (2–15 October). The stable high-NO_x (winter) and low-NO_x (summer) regions are separated by sequences of unstable states shown in red. The instability in the steady-state mode corresponds relatively well to the times at which the dominant pathway for OH reaction, Fig. 3c, switches from nitric acid formation to hydrocarbon oxidation in the spring (day 80, 21 March) and back to nitric acid formation in the fall (day 290, 17 October). The spring increase in time-dependent mixing ratio, Fig. 3b, is most rapid between days 78 and 86 (19–27 March) in reasonable agreement with the switch from high to low-NO_x conditions indicated by the steady-state model (Fig. 3a) and the comparison of OH reaction rates (Fig. 3c). During this time the peroxide mixing ratio increases from about 1 ppt to 300 ppt. Thereafter a slower increase to the summer maximum of about 2.5 ppb takes place. In the fall, the most rapid decrease in peroxide mixing ratio occurs between days 280 and 310 (2 October to 6 November) and is roughly the opposite of the spring increase, but over a longer time span. HO_2 loss rates shown in Fig. 3d indicate that the summer low-NO_x regime is ozone producing throughout. It also indicates, in contrast with the model in Fig. 2, that significant H_2O_2 production occurs only in summer.

As S_{NO} is increased from the value used in Fig. 3, the bistable regions in the steady-state calculation lengthen and the neck of the mushroom is pinched inward.

The changes resulting from further increase in S_{NO} are seen in Fig. 4a where the spring and fall bistable regions extend from days 95 to 158 (5 April to 7 June) and 205 to 268 (24 July to 25 September). The NO source used in the model shown in Fig. 4 is $S_{NO}=3.73\times10^6$. This value is chosen for display since it is the highest S_{NO} considered for which the time-dependent model shows high to low-NO_x transitions.

It is a consequence of the model design that the steady-state profile is symmetric about mid-summer. However, the steady-state calculation suggests that its time-dependent analogue will not be. As days progress through the seasons, a transition from winter to summer conditions will not be forced until 7 June and the corresponding return to winter not forced until 25 September. We thus expect a shift of the time-dependent profile towards the fall side of summer, the shift being greater the more pronounced the pinch in the neck of the mushroom. This is apparent in Fig. 4b along with a much more dramatic asymmetry in the rates of the spring increase and fall decrease of $[H_2O_2]$. The high to low-NO_x transition in the time-dependent H_2O_2 profile begins on day 195 (14 July) and is completed in 3 days. The mixing ratio increase

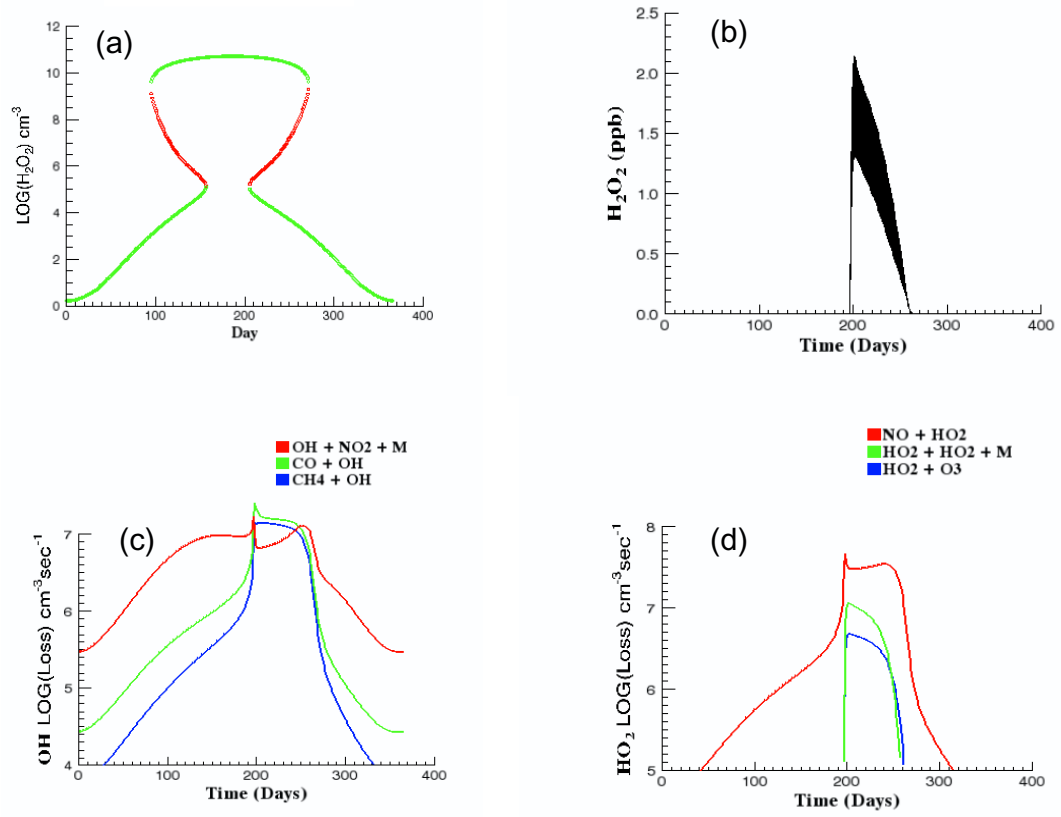

Fig. 4. Similar to Figs. 2 and 3, but with an assumed S_{NO} of 3.73×10^6 cm^{-3} s^{-1}. The summer to winter range of NO_x is 2 to 70 ppb. Part **(c)** shows that HNO_3 formation (now in red) dominates CO (green) and CH_4 (blue) oxidation except for a brief period of about 52 days in summer. In panel (d) the dominance of HO_2 reaction with NO (red) rather than O_3 (blue) facilitates ozone production in the low NO_x regime.

in this period is from 0.5 ppt to 1.7 ppb. The much less abrupt fall transition occurs between days 250 and 280 (7 September to 7 October). The mixing ratio decreases from 0.4 ppb to 0.002 ppt during this 30 day interval. The difference in rapidity of spring and fall transitions is a consequence of the different mechanisms involved in H_2O_2 production (spring) and loss (fall) mechanisms. In spring, peroxide production is limited by the rapid radical reactions in the chain propagation phase, Reactions (3–5) in Sect. 2.1. In the fall its loss is limited by photolysis and reaction with the OH radical. These loss reactions are included in the model, but are not part of the simplified scheme given by Reactions (1) to (7). The switch between nitric acid formation and hydrocarbon (CO and CH_4) oxidation by OH occurs on days 195 and 248 (Fig. 4c) corresponding to the transitions described for the H_2O_2 mixing ratio. The chemistry, as expected, is ozone producing throughout the short low-NO_x portion of summer (Fig. 4d). The NO_x range in this model is about 70 ppb (winter/spring) to 2 ppb (summer), characteristic of rural to urban-suburban regions (National Research Council, 1992). The correspondence between steady-state and time-dependent models in the time of the spring transition is not as close as that shown in Fig. 3. Although, according to the steady-state model, a transition should be forced by 7 June it does not occur in the time-dependent case until 14 July.

Figure 5 shows the model calculations for $S_{NO}=4.0\times10^6$ cm^{-3} s^{-1} and a corresponding summer to winter [NO_x] of 75 to 130 ppb. This is the next higher source value from that considered in Fig. 4. The mushroom configuration seen in Fig. 3a and 4a has now become a continuous branch of high NO_x states (Fig. 5a) that persists throughout the year and an isolated branch consisting of low-NO_x summer values and unstable states. An isolated branch of solutions as shown in Fig. 5a is called an "isola" (Grey and Scott, 1990).

For this and higher NO source and [NO_x] background values, the summer low-NO_x states are inaccessible from the time-dependent model. This model remains in a high-NO_x state throughout the year as indicated by the low H_2O_2 mixing ratios (Fig. 5b) and the dominance of nitric acid formation over hydrocarbon oxidation (Fig. 5c). The units in Fig. 5b are parts per quadrillion (ppqd). The HO_2 ozone Production/Loss switch remains in the production position (Figs. 5d and 1), but this is irrelevant since oxidant

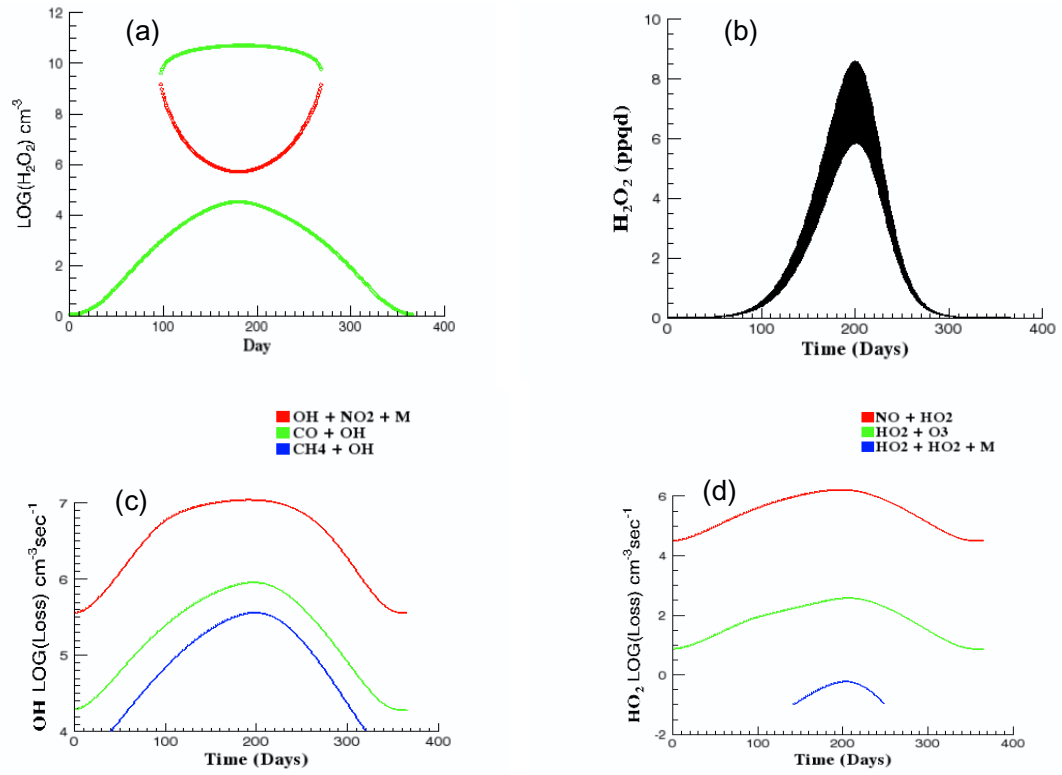

Fig. 5. Similar to Figs. 2–5 but for an assumed $S_{NO}=4.0\times10^6\,cm^{-3}\,s^{-1}$. The summer to winter NO_x range is 75 to 130 ppb. The OH reaction rates in part **(c)** indicate high-NO_x dominance throughout the year. In this high-NO_x regime H_2O_2 production is negligible **(d)**.

production has been effectively cut off by the switch from low to high-NO_x chemistry (Fig. 1, OH box). Figure 5d shows the negligible peroxide production rate. As S_{NO} increases further, the isola shown in Fig. 5a shrinks and finally disappears at $S_{NO}\approx1.5\times10^7\,cm^{-3}\,s^{-1}$.

The NO_x mixing ratios in this model are characteristic of the urban troposphere (National Research Council, 1992), but the overall model chemistry is not since no significant NMHC are included. In a more comprehensive chemical model, NMHC would result in greater HO_x production and defer an annually dominant high-NO_x regime to higher background NO_x levels. For example, the model study of Honoré et al. (2000) contains a more realistic urban chemistry. These authors employ a chemistry-transport box model and, for stagnant conditions, find two distinct diurnal equilibria for NO_x emissions $\sim$ a few times $10^7\,cm^{-3}\,s^{-1}$ (this estimate is based on their reported maximum NO_x emissions, NO_x emission weight and their maximum mixed layer height of 1.5 km). Their bistable regime occurs at NO_x source values that would result in only high-NO_x solutions in the current model. This effect is also seen in many other models of urban photochemistry in which contour plots of O_3 (or O_3 production) as a function of NO_x and VOC (volatile organic compounds) mixing ratios show the low-NO_x (or NO_x-sensitive or NO_x-limited) to high-NO_x (or VOC-sensitive or VOC-limited) transition moving to higher NO_x values as VOC increases. Examples may be found in Sillman (1999) and Tonnesen (1999).

The progression of steady-state solutions shown in Figs. 2a–5a are slices through a three-dimensional (Day, S_{NO}, $[H_2O_2]$) surface for selected (Day, $[H_2O_2]$) planes perpendicular to the NO source axis. The full set of solutions is shown by the bifurcation surface in Fig. 6. In this figure the Day axis ranges from days 0 through 400 increasing away from the vertex. The NO source axis, labeled $Log(S/cm^3*s)$, ranges from 8 to 4 decreasing away from the vertex and the $Log(H_2O_2/cm^3)$ concentrations range through twelve orders of magnitude. The top part of this figure, furthest from the day axis, represents the purely low-NO_x solutions corresponding to situations like that shown in Fig. 2a. Since the annual range of low-NO_x peroxide values is only about 2 ppb, this portion of Fig. 6 has a flat appearance. Slices taken with a plane parallel to the plane defined by the (Day, $Log(H_2O_2)$) axes generate the profiles in Figs. 2a through 5a. The rightmost such plane generates the purely low-NO_x profile of Fig. 2a. As this plane is moved towards the front of the figure, the pure low-NO_x solutions give way to mushrooms with increasingly pinched necks, then to a combination of high-NO_x solution branches and low-NO_x isolas and finally to a single branch of high-NO_x solutions. These last are along the lower part of the figure nearest the day axis.

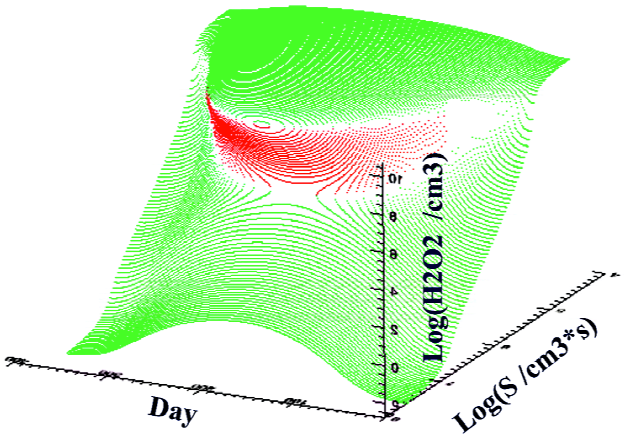

Fig. 6. H_2O_2 bifurcation surface. Selected slices through this surface parallel to the plane defined by the Day, Log(H_2O_2) axes generate the profiles shown in Figs. 2–5.

As stated in the preceding text, to test the robustness of the results some runs have been made with changes in selected parameter values and model reactions. Interesting variants on the above model are provided by cases in which, as S_{NO} is increased from low values, a high-NO_x isola, lying under the branch of low-NO_x states, first develops in winter. This isola grows and merges with the low-NO_x states to form a single mushroom branch, similar to Figs. 3a and 4a. The neck of the mushroom then pinches off to leave a continuous branch of high-NO_x states and a low-NO_x summer isola as in Fig. 5a. An example of such a system is a model consisting only of Reactions (1–7) supplemented by HNO_3 deposition and H_2O_2 deposition, photolysis and reaction with OH. The results regarding the correspondence between steady-state bifurcations and time-dependent transitions in the model remain unaltered.

3.2 Annual Variation of Selected Species

Table 3 shows the approximate winter to summer change in noon mixing ratio for selected species in the time-dependent models shown in Figs. 2b–5b. The corresponding labels in the table are F2–F5. These models are characterized by increasing assumed NO source values and hence by increasing NO_x mixing ratios.

Model F2 is typical of a low-NO_x, ozone destruction environment. Ozone in this case is higher in winter than summer since the enhanced summer photolysis acts to destroy it. This type of annual ozone cycle is seen in the remote marine troposphere at Cape Grim (Ayers et al., 1996). In this environment the seasonal variation of O_3 is negatively correlated with H_2O_2 and positively correlated with CO.

Table 3. Average winter (W) and summer (S) values in selected species mixing ratios (all in ppb). Models F2 through F5 correspond to the calculations shown in Figs. 2–5.

Model	F2		F3		F4		F5	
Season	W	S	W	S	W	S	W	S
O_3	75	55	70	85	20	100	40	40
NO_x	.08	.04	5	0.5	70	2	130	75
CO	95	70	90	55	130	55	130	125

4 Discussion

As noted in the introduction to the paper, there are two sets of H_2O_2 measurements that cover one or more annual cycles and are thus of particular interest to this model study. One of these is the Cape Grim, Tasmania measurements of Ayers et al. (1996), the other the measurements of Sakugawa and Kaplan (1989) at Westwood, CA in the Los Angeles basin. These clearly represent different pollution backgrounds. The Cape Grim observations are characteristic of clean maritime air while those near Los Angeles are more polluted having mean NO_x over the measurement period of 36 ppb.

The Cape Grim measurements are presented as hourly average concentrations of total peroxide between early February 1991 and late March 1992. The monthly mean concentrations show a seasonal cycle with a range of values from ∼200 ppt in winter to 1.4 ppb in summer. The background atmosphere is low-NO_x, ozone-destroying throughout the year as evidenced by the high winter and low summer ozone concentrations. These data are thus comparable to the low-NO_x cycle shown in Fig. 2. The summer maximum in Fig. 2b is larger than that in the Cape Grim data, 2 ppb of H_2O_2 as compared to the monthly mean 1.4 ppb total peroxide. Maximum total peroxide concentrations during summer at Cape Grim did sometimes exceed 2 ppb. The NO concentrations during the measurement period are unknown, but a value of 3 ppt was assumed by Ayers et al. (1996) in modeling their data. If this is reasonably accurate then the range of 40 to 80 ppt in the model shown in Fig. 2 would be expected to result in higher peroxide. The principal feature to note in both the model and data is the lack of a sharp winter/summer transition in H_2O_2 concentrations. The Cape Grim monthly mean peroxide values as well as the model calculations presented by the authors, both shown in their Fig. 4, show a gradual rise from the July winter low to the December summer high concentrations. The change may be described as following a more or less sinusoidal curve.

The Sakugawa and Kaplan data cover the annual variation of H_2O_2 over three years from August 1985 through September 1988 at Westwood, CA. Two complete annual cycles for years 1986 and 1987 are shown as well as part of the 1985 and 1988 cycles. The H_2O_2 concentrations are 4-hour averages (1200–1600 hr) taken on selected days (clear to partly

cloudy skies) during each month. Mean, maximum and minimum values of NO_x, NMHC and other pollutants over the entire observation period are reported. The mean NO_x level of 36 ppb is within the range of values in the model calculations shown in Figs. 3 and 4. In contrast to the Cape Grim data and the low-NO_x cycle shown in Fig. 2, the Westwood cycles show rapid changes between winter and summer conditions, especially in the spring. For example, the 1986 [H_2O_2] values remain relatively low until June at which time a change to summer concentrations occurs. The temporal resolution of the data doesn't permit an evaluation of the time taken for this transition, but it is clearly completed in the month of June. The summer data for this particular year are sparse, but the return to winter concentrations is completed by the beginning of September. The overall appearance of this cycle is that of a "spike", sharper than the model profile in Fig. 4b. There is no obvious difference in the rapidity of spring and fall transitions in the 1986 cycle, but there are fewer data points by which to judge than in the following year. The 1987 cycle also shows a rapid winter to summer transition beginning in April with some high H_2O_2 values extending into October. Here, there is a suggestion of a difference in rapidity with which the spring and fall transitions occur with high H_2O_2 values extending, with decreasing frequency, into October.

Some features of the Sakugawa and Kaplan time series differ from the profiles shown in Figs. 3 and 4 in the present model. Foremost among these is the range of winter to summer values. Observed summer [H_2O_2] had a mean value $\sim$1.0 ppb while the model calculations reach or exceed 2 ppb in any model with a low-NO_x summer. Observed winter [H_2O_2] had a mean value $\sim$0.2 ppb whereas it is essentially 0 in the model calculations with a high-NO_x winter. Since the NMHC chemistry considered in the model is limited it is probable that winter production of H_2O_2 resulting from NMHC oxidation by O_3 and NO_3 is underestimated. In a model study based on Westwood conditions Sakugawa et al. (1990) calculated maximum H_2O_2 concentrations of $\sim$3.2 ppb in summer (July) and 0.05 ppb in winter (January).

The Westwood CA data do not contain enough information to calculate radical production and loss rates like those carried out by Kleinman (1991) thus confirming a high-NO_x winter to low-NO_x summer transition. Nonetheless, the morphological differences in the clean air Cape Grim observations and the more polluted Westwood observations and the similar changes in model profiles shown in this paper as NO_x background increases (Figs. 2b through 4b) suggest that such transitions occur.

5 Summary and conclusions

This paper has explored the relationship between the chemical instability seen in steady-state tropospheric models and corresponding time-dependent behavior. The objective has been to see whether the observed changes in H_2O_2 concentrations from summer to winter may, under some circumstances, be interpreted as a manifestation of chemical instability. The main features shown by the model calculations are the following: first, an increase in the sharpness of the winter high-NO_x to summer low-NO_x transition as NO_x concentration increases; second, an asymmetry in both rapidity and time of the spring and fall transitions, the time of transition shifting towards the fall side of summer as NO_x levels increase; and third, a correspondence between time-dependent high/low NO_x transitions and instability in the underlying (steady-state) chemistry.

The data sets discussed above lend support to the first of these features. The change from winter low to summer high peroxide concentrations is much more gradual in the clean air observations of Ayers et al. (1996) than in the Sakugawa and Kaplan (1989) observations near Los Angeles. The 1987 annual cycle observed by Sakugawa and Kaplan (1989) are compatible with the second feature, but this is less clear in the 1986 cycle. Finally, the third feature would require additional observations sufficient to calculate radical production and loss rates. The correspondence cited in the third feature is not an observable, but is important in interpreting observations of change in peroxide concentrations as indicative of bistability in the chemical system.

The rapid growth of [H_2O_2] predicted for spring high to low-NO_x transitions would be a more definitive indicator of instability than would the slower [H_2O_2] decay in the fall low to high-NO_x transition. Shorter transition times correspond to higher S_{NO}, and thus higher background NO_x values. For NO source values greater than 2×10^6 cm^{-3} s^{-1}, the spring transition in the model reported here results in [H_2O_2] increases from $<$10 ppt (i.e. unobservable) to a few hundred ppt in periods of 3 to 7 days. Ideally, observations would be carried out over one or more annual cycles in a region in which winter [NO_x] is sufficient to govern a high-NO_x regime. A persistent interval, days to weeks, of below detection limit to perhaps tens of ppt peroxide concentrations followed by a change over an interval of a week or less to a period of detectable and rapidly increasing concentrations would suggest that bifurcations in the chemistry might be invoked as an explanation. On the other hand, a relatively smooth transition such as that shown in the Cape Grim data (Ayers et al., 1996) or in the model profile of Fig. 2b would indicate that such a nonlinear effect does not occur. If the observed data set included additional observations sufficient to compute radical production and loss rates, CO, CH_4, NMHC, O_3, H_2O, and NO_x, as well as meteorological variables, a definitive conclusion might be possible.

The model used in this study, in common with many models, gives results that are concise and readily interpretable. Nature is not so accommodating. Clouds and fogs form and dissipate, rain falls and winds blow. All such events influence the concentration of a moderately long-lived and soluble species such as H_2O_2. The result is a degree of variability that is sure to complicate any attempt to relate observations

to the consequences of chemical influences. The greatest difficulty in carrying out a program of H_2O_2 observations would probably be separating the effects of transport from local photochemistry. However, although the Sakugawa and Kaplan (1989) observations show considerable scatter, there is a clear winter/summer separation so the possibility of using such measurements, along with the additional observations noted above, to definitively establish instability or its absence in atmospheric photochemistry cannot be ruled out. Should difficulties in using H_2O_2 prove insurmountable it might still be possible to look for evidence of chemical instability in the transitions of a shorter-lived species, such as OH, that would quickly relax to the local chemistry following transport events.

Chemical instability is a mathematical characteristic of photochemical models. Due to the magnitude of the changes induced by such instability the question of the existence of atmospheric consequences should be pursued.

Edited by: P. Monks

References

Atkinson, R., Baulch, D. L., Hampson , R. F. Jr., Kerr, J. A., and Troe, J.: Evaluated kinetic and photochemical data for atmospheric chemistry, J. Phys. Chem. Ref. Data 21, suppl. IV, 1125–1568, 1992.

Ayers, G. P., Penkett, S. A., Gillett, R. W., Bandy, B., Galbally, I. E., Meyer, C. P., Ellsworth, C. M., Bentley, S. T., and Forgan, B. W.: The annual cycle of peroxides and ozone in marine air at Cape Grim, Tasmania, J. Atmos. Chem., 23, 221–252, 1996.

Barker, J. R.: A Brief Introduction to Atmospheric Chemistry, in Progress and Problems, in Atmospheric Chemistry, edited by Barker, J. R., pp. 1–33, World Scientific, Singapore, 1995.

Bottenheim, J. W. and Shepherd, M. F.: C_2–C_6 Hydrocarbon measurements at four rural locations across Canada, Atmos. Environ., 29, 647–664, 1995.

Crutzen, P. J. and Zimmermann, P. H.: The changing photochemistry of the troposphere, Tellus, 43AB, 136–151, 1991.

DeMore, W. B., Sander, S. P., Golden, D. M., Hampson, R. F., Kurylo, M. J., Howard, C. J., Ravishankara, A. R., Kolb, C. E., and Molina, M. J.: Chemical kinetics and photochemical data for use in stratospheric modeling, JPL publication 97-4, 1997.

Dimitroulopoulou, C. and Marsh, A. R. W.: Modelling studies of NO_3 nighttime chemistry and its effects on subsequent ozone formation, Atmos. Environ., 31, 3041–3057, 1997.

Field, R. J., Hess, P. G., Kalachev, L. V., and Madronich, S.: Characterization of oscillation and a period-doubling transition to chaos reflecting dynamic instability in a simplified model of tropospheric chemistry, J. Geophys. Res., 102D, 7553–7565, 2001.

Fox, J. L., Wofsy, S. C., McElroy, M. B., and Prather, M. J.: A Stratospheric Chemical Instability, J. Geophys. Res., 87, 11 126–11 132, 1982.

Gnauk, T., Rolle, W., and Spindler, G.: Diurnal variations of atmospheric hydrogen peroxide concentrations in Saxony (Germany), J. Atmos. Chem., 27, 79–103, 1997.

Grey, P. and Scott, S. K.: Chemical Oscillations and Instabilities: Non-linear Chemical Kinetics, Oxford Science Publications, New York, 1990.

Hameed, S., Pinto, J. P., and Stewart, R. W.: Sensitivity of the Predicted CO-OH-CH_4 Perturbation to Tropospheric NO_x Concentrations, J. Geophys. Res., 84, 763–768, 1979.

Hauglustaine, D. A., Granier, C. Brasseur, G. P., and Megie, G.: The importance of atmospheric chemistry in the calculation of radiative forcing on the climate system, J. Geophys. Res., 99, 1173–1186, 1994.

Hindmarsh, A. C.: Odepack, a systematized collection of ode solvers, in Scientific Computing, edited by Stepleman, R. S., et al., pp. 55–64, North-Holland, Amsterdam, 1983.

Holton, J. R. and Lelieveld, J.: Stratosphere-Troposphere Exchange and its role in the budget of tropospheric ozone, in Proceedings of the NATO Advanced Research Workshop, Clouds, Chemistry and Climate, edited by Crutzen, P. and Ramanathan, V., pp. 173–190, Ringberg, Germany, 1994.

Honoré, C., Vautard, R., and Beekmann, M.: Photochemical regimes in urban atmospheres: The influence of dispersion, Geophys. Res. Lett., 27, 1895–1898, 2000.

Jacob, D. J., Horowitz, L. W., Munger, J. W., Heikes, B. G., Dickerson, R. R., Artz, R. S., and Keene, W. C.: Seasonal transition from NO_x to hydrocarbon-limited conditions for ozone production over the eastern United States in September, J. Geophys. Res., 100, 9315–9325, 1995.

Kalachev, L. V. and Field, R. J.: Reduction of a model describing ozone oscillations in the troposphere, J. Atmos. Chem., 39, 65–93, 2001.

Kleinman, L. I.: Seasonal Dependence of Boundary Layer Peroxide Concentrations: The Low and High NO_X Regimes, J. Geophys. Res., 96, 20 721–20 733, 1991.

Kleinman, L. I.: Low and High NO_x tropospheric photochemistry, J. Geophys. Res., 99, 16 831–16 838, 1994.

Konovalov, I. B., Feigin, A. M., and Mukhina, A. Y.: Toward understanding of the nonlinear nature of atmospheric photochemistry: Multiple equilibrium states in the high-latitude lower stratosphere photochemical system, J. Geophys. Res., 104, 3669–3689, 1999.

Lee, M., Heikes, B. G., and O'Sullivan, D. W.: Hydrogen peroxide and organic hydroperoxide in the troposphere: a review, Atmos. Environ., 34, 3475–3494, 2000.

Lelieveld, J., Peters, W., Dentener, F. J., and Krol, M. C.: Stability of tropospheric hydroxyl chemistry, J. Geophys. Res., 107(D23) doi:10.1029/2002JD002272, 2002.

Levy, H.: Normal atmosphere: Large radical and formaldehyde concentrations predicted, Science, 173, 141–143, 1971.

Madronich, S.: Photodissociation in the atmosphere 1. Actinic flux and the effect of ground reflectance and clouds, J. Geophys. Res., 92, 9740–9752, 1987.

National Research Council: Rethinking the ozone problem in urban and regional air pollution, National Academy Press, Washington D.C., 1992.

Olivier, J. G. J., Bloos, J. P. J., Berdowski, J. J. M., Visschedijk, A. J. H., and Bouwman, A. F.: A 1990 global emission inventory of anthropogenic sources of carbon monoxide on $1^\circ \times 1^\circ$ developed in the framework of EDGAR/GEIA, Chemosphere: Global Change Science, 1, 1–17, 1999.

Paulson, S. E.: The Tropospheric Oxidation of Organic Compounds: Recent developments in OH, O_3, and NO_3 Reactions with Isoprene and Other Hydrocarbons, in Progress and Problems in Atmospheric Chemistry, edited by Barker, J. R., pp. 111–144, World Scientific, Singapore, 1995.

Poppe, D., Wallasch, M., and Zimmermann, J.: The dependence of the concentration of OH on its precursors under moderately polluted conditions: a model study, J. Atmos. Chem., 16, 61–78, 1993.

Prather, M. J., McElroy, M. B., Wofsy, S. C., and Logan, J. A.: Stratospheric Chemistry: Multiple Solutions, Geophys. Res. Lett., 6, 163–164, 1979.

Prather, M. J.: Lifetimes and eigenstates in atmospheric chemistry, Geophys. Res. Lett., 21, 801–804, 1994.

Press, W. H., Teukolsky, S. A. Vetterling, W. T., and Flannery, B. P.: Numerical Recipes in FORTRAN The Art of Scientific Computing, 2nd Ed., Cambridge University Press, United Kingdom, 1992.

Sakugawa, H. and Kaplan, I. R.: H_2O_2 and O_3 in the atmosphere of Los Angeles and its vicinity: factors controlling their formation and their role as oxidants of SO_2, J. Geophys. Res., 94, 12 957–12 973, 1989.

Sakugawa, H., Wangteng, T., Kaplan, I. R., and Cohen, Y.: Factors controlling the photochemical generation of gaseous H_2O_2 in the Los Angeles Atmosphere, Geophys. Res. Lett., 17, 93–96, 1990.

Sander, S. P., Friedl, R. R., Golden, D. M., Kurylo, M. J., Huie, R. E., Orkin, V. L., Moortgat, G. K., Ravishankara, A. R., Kolb, C.E., Molina, M. J., and Finlayson-Pitts, B. J.: Chemical Kinetics and Photochemical Data for Use in Atmospheric Studies, Evaluation Number 14, JPL Publication 02-25, 2003.

Sillman, S.: The relation between ozone, NO_x, and hydrocarbons in urban and polluted rural environments, Atmos. Environ., 33, 1821–1845, 1999.

Snow, J. A., Heikes, B. G., Merrill, J. T., Wimmers, A. J., Moody, J. L., and Cantrell, C. A.: Winter-spring evolution and variability of HO_x reservoir species, hydrogen peroxide and methyl hydroperoxide, in the northern middle to high latitudes, J. Geophys. Res., 108(D4) doi:10.1029/2002JD002172, 2003.

Stewart, R. W., Hameed, S., and Pinto, J. P.: Photochemistry of tropospheric ozone, J. Geophys. Res., 82, 3134–3140, 1977.

Stewart, R. W., Hameed, S., and Matloff, G.: A model study of the effects of intermittent loss on odd nitrogen concentrations in the lower troposphere, J. Geophys. Res., 88, 10 697–10 707, 1983.

Stewart, R. W.: Multiple steady states in atmospheric chemistry, J. Geophys. Res., 98, 20 601–20 611, 1993.

Stewart, R. W.: Dynamics of the low to high NO_x transition in a simplified tropospheric photochemical model, J. Geophys. Res., 100, 8929–8943, 1995.

Tie, X., Emmons, L., Horowitz, L., Brasseur, G., Ridley, B., Atlas, E., Stround, C., Hess, P., Klonecki, A., Madronich, S., Talbot, R., and Dibb, J.: Effect of sulfate aerosol on tropospheric NO_x and ozone budgets: Model simulations and TOPSE evidence, J. Geophys. Res., 108(D4), 8364, doi:10.1029/2001JD001508, 2003.

Tinsley, M. R. and Field, R. J.: Dynamic instability in tropospheric photochemistry: An excitability threshold, Geophys. Res. Lett., 28, 4437–4440, 2001.

Tonnesen, G. S.: Effects of uncertainty in the reaction of the hydroxyl radical with nitrogen dioxide on model-simulated ozone control strategies, Atmos. Environ., 33, 1587–1598, 1999.

White, W. H. and Dietz, D.: Does the photochemistry of the troposphere admit more than one steady state?, Nature, 309, 242–244, 1984.

Yang, P. and Brasseur, G.: Dynamics of the oxygen-hydrogen system in the mesosphere 1. Photochemical equilibria and catastrophe, J. Geophys. Res., 99, 20 955–20 965, 1994.